



# Coal and Rock Classification with Rib Images and Machine Learning Techniques

Yuting Xue<sup>1</sup>

Received: 1 October 2020 / Accepted: 6 December 2021 / Published online: 13 January 2022

This is a U.S. government work and not under copyright protection in the U.S.; foreign copyright protection may apply 2021

## Abstract

Classification of rock and coal is one preliminary problem for fully automated or intelligent mining. It assists for the automated rib stability analysis and enables the shearer to adjust the drums without human intervention. In this paper, the classification of rock from coal on rib images has been studied with machine learning techniques. A database of rock and coal image has been created by filtering photographs taken by NIOSH researchers in gateroad during site visits and only the images with fresh areas of rock and coal on the rib were selected. Machine learning was conducted on patches with a determined size, which are smaller images randomly extracted from each rock or coal image. After training, the classifier was validated with the testing dataset and an accuracy score of 0.9 was obtained. The influence of patch size and classifier was also investigated. The trained classifier was then applied to classify rock and coal on a new rib image with three rock layers of different thicknesses and good agreement was achieved.

**Keywords** Rock classification · Image processing · Patch · Machine learning · SVM · Random forest

## 1 Introduction

The failure of coal pillar ribs is a major hazard in underground coal mines. Over the past decade, rib falls resulted in 16 fatalities, representing over 50% of the ground-fall fatalities in U.S. underground coal mines. More recently, the falls of rib or face led to all three fatalities resulted from ground fall in 2018 and 2019. It clearly indicates that rib or face falls are contributing more to mineworker fatalities than any other ground-fall fatality cause [1]. Extensive studies have been conducted to identify contributing factors, to develop analysis method and to design rib support [2–8]. To eliminate injury and fatality due to rib falls in underground coal mines, the National Institute for Occupational Safety and Health (NIOSH) researchers are currently working on the development of a Coal Pillar Rib Rating (CPRR) technique to quantify the bearing capacity of coal pillar ribs [1].

At the same time, the need to improve mining efficiency and productivity and to increase personnel safety has been the primary drive for the global coal mining industry. The

ongoing development and implementation of automation technology has significant potential to provide meaningful solutions by facilitating more accurate mining methods, incorporating sensing to optimally control equipment, and increasing personnel safety through remote process operation [9]. The application of the automation techniques for coal rib rating will significantly facilitate the coal rib rating process in underground coal mines.

Three main rib categories could be observed in underground coal mines, including (a) solid coal rib with or without thin partings of thickness under 50 mm, (b) coal rib with an in-seam rock parting of thickness greater than 0.15 m, and (c) coal rib with a roof brow [10]. The first case has been extensively studied and a rib rating technique has been developed for solid coal ribs [1]. The rib rating techniques for the other two cases involving rock partings in the coal ribs are under development [11]. When there are rock partings, the presence, location and thickness of the rock parting will affect the failure modes and bearing capacities of the coal ribs [6, 12]. Depending on the presence and location of the rock partings, different adjustments will be conducted for the rib rating. Thus, the first step of coal rib rating is to classify rock from the coal ribs.

The classification of rock and coal on ribs has been applied for shearer horizon control at longwall mining

✉ Yuting Xue  
qcj1@cdc.gov

<sup>1</sup> CDC NIOSH Pittsburgh Mining Research Division,  
Pittsburgh, PA, USA

face. It provides the information for the shearer to adjust the cutting drums. An automated shearer will cut the coal and stay in-seam without the need for human intervention [13]. Besides knowing the shearer's location, direction, and speed of travel, the shearers need to know the elevation of the drums with respect to the roof/coal interface. The classification of rock and coal at the mining face enables the shearer to automatically track the interface between rock and coal. Different methods have been proposed and applied for the detection of rock-coal interfaces at longwall faces based on different properties of coal. The "memory cut" technique records the data on drum elevation, ranging arm inclination, and shearer location during the training run and recalls the data to run the subsequent shearer's cuts [14]. This technique has been improved substantially since its introduction and has been widely used for automated shearers with the help of various sensors. However, operators are required when a new training run is necessary. Gamma-ray coal thickness sensors, which only work in shale roof, have also been used to detect the rock-coal interface through coal thickness measurement [15]. In the inertia navigation system (INS), a thermal infrared camera was used for shearer's horizon control through detecting the heating of marker bands in the coal seam [16]. INS has been widely used in Australian coal industry, but it was only recently introduced into US longwall mining [13]. Cutting signal and infrared thermography were also used to identify rock and coal based on the tests with different proportions of rock-coal mixture [17, 18]. Miao et al. used ground penetrating radar (GPR) as a non-contacting approach for detecting rock and coal by interpreting the radar images [19].

Image processing is another method applied to classify rock and coal. Generally, it is a classification problem where images are used to classify different rock types. The rationale behind this technique is that rocks can be distinguished by the difference in particle size, composition, color, and structure, which are general reflections of the mineral and chemical composition, formation environment, and genesis of the rocks. These features can all be captured with images. When exploiting the sensitivity of the human visual system to texture, Rao and Lohse found that the most important textural features in the natural texture perception are repetitiveness, directionality, and granularity. The texture of a rock is the size, shape, and arrangement of the grains [20]. The visual texture contains variations of intensities, forming certain repeated patterns. However, the differences observed by visual inspection, which are stochastic in nature, are difficult to define in a quantitative manner. Partio et al. used the gray level co-occurrence matrix (GLCM) to automatically retrieve texture for rock image [21]. This method was also used by Sun and Su to extract image features of rock and coal for rock and coal classification [22]. Lepistö et al. tried to retrieve and classify rock images based on various texture

features, including granularity [23], directionality [24], and color [25]. Microscopy image analysis has also been used to characterize coal lithotypes and perform automated lithotype analyses on coal samples [26–29].

In addition, machine learning techniques have been used for rock classification with images. Machine learning is the field of study that gives computers the ability to learn without being explicitly programmed [30]. Machine learning is fundamentally based on statistical methods. The advantage is that machine learning can be applied to dig into a large amount of data and help discover patterns that are not immediately apparent [31]. Ran et al. classified rock types from field images with a deep convolutional neural network [32]. In this research, a deep learning model was trained with the digital images taken from a field site, and the images include six rock types (mylonite, granite, conglomerate, sandstone, shale, and limestone) with these rocks having a clear difference in grain size, distribution, structure, and color. The results demonstrate the potential of using rock images to classify the rock types with machine learning.

In this paper, machine learning techniques were applied for the classification of rock and coal from rib images. The storage of digital images in Python and the potential mechanisms for image classification were first introduced to provide a big picture of how the classification of rock types is achieved based on digital images. Following this step, the preprocessing of field images and the collected rock and image database were then summarized. Image patches were further extracted from the rock and coal images to generate a database of patches, which are the subjects for machine learning. Various techniques for machine learning were used to preprocess the data, enhance the speed of the process, and increase the accuracy. The influence of patch size and classifier was also investigated. Finally, the trained classifier was applied on a new rib image for rock and coal recognition.

## 2 Machine Learning with Images and the Image Database

### 2.1 Image Storage in Python

Each image or photo is made up of pixels in digital form. Pixels are the smallest unit of image information. The value for each pixel represents the intensity of a color and varies from 0 to 255, indicating that there are potentially 256 different intensity values. For RGB images, there are three color channels, namely red, green, and blue, which make each pixel have three layers or components. There are different pixel values within each color channel. The pixel values in three color channels combine to generate the pixel we normally observe. This indicates that, for one color pixel, there are 16.8 million ( $256 \times 256 \times 256$ )

possibilities or combinations. An RGB image was decomposed into three color channels in Python and is shown in Fig. 1. We can see that, at the same locations on the image, the brightness or pixel value varies with the color channels.

As shown in Fig. 1, the image is represented by a matrix of pixels for each color channel, and the pixel matrixes resulted from different color channels are stored in the third dimension. This means that an RGB image has three layers, and each layer is a matrix of pixels. Therefore, an RGB image is stored as a three-dimensional array. In contrast, gray images, which contain only black and white, are stored as a two-dimensional array and there is no third dimension for different color channels. In summary, an image can be treated as numerical data in the form of two- or three-dimensional arrays in Python. This makes it possible to analyze the features of the images, like color, grain size, and structure, through numerical data.

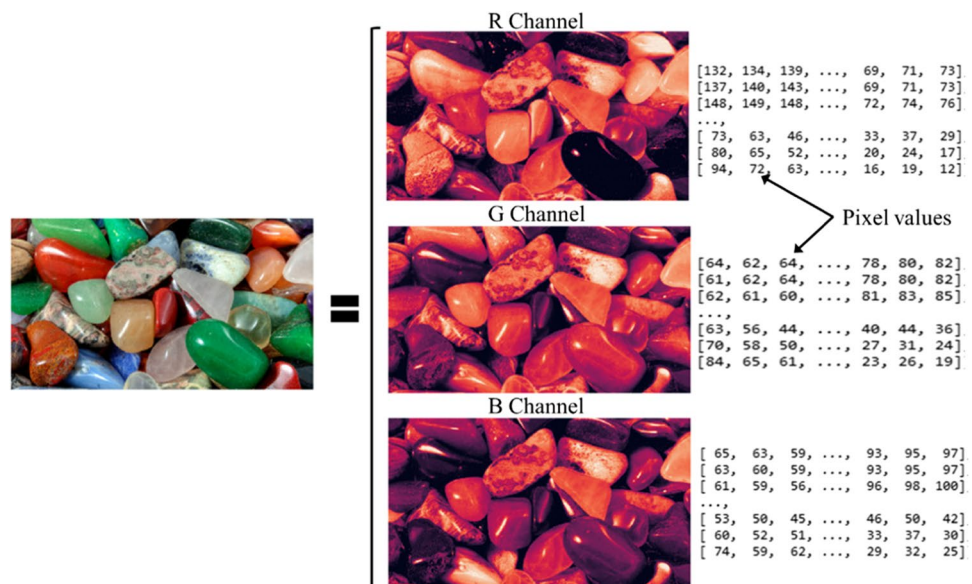
The size of the pixel matrixes depends on the dimension of pixels in any given image, which is basically the number of pixels along the horizontal and vertical direction in the image. With a dimension of 50\*50 in pixels, the image has 50 pixels in height (vertical) and 50 pixels in width (horizontal). This is the size of the matrix in one layer. They have the same dimensions, but different pixel values in the other two color-channels. For an RGB image, the total pixel number is 50\*50\*3. Each pixel value can be used as one feature of the image for machine learning, and thus, the number of features for the image is 7,500.

## 2.2 Potential Mechanism for Rock and Coal Classification

Coal and other coal measures rocks are sedimentary rocks. They are formed by the accumulation of sediments on or near the Earth's surface. The difference in composition and sedimentary environment provides some unique features to classify coal and other coal measures rocks. Coal is an organic sedimentary rock that is formed when plant material is buried under sediments over millions of years. The decomposing vegetation was converted into peat and then into coal under immense pressure. The organic material cannot decay under anoxic circumstances and leaves a dark sediment. The gray and black colors mostly result from partially decayed organic matter. Due to the rich in organic material, coal is commonly black. The color provides an approach to classify coal from some coal measures rocks, which are not black.

In addition, most coal seams are extensively naturally fractured or cleated. Coal, at the very beginning of formation, had a high moisture content, which progressively decreases as rank increases. The dehydration process tends to increase coal fractures. In addition, the loss of volatile matter occurs during the coalification process and produces a decrease in coal volume. This further induces fractures in coal seam. Tectonics controls cleat orientation in coal in a process somewhat similar to jointing observed in other rocks [34]. The cleat system is normally characterized by two main sets of fractures. Face cleats are usually dominant with individual surfaces almost planar, persistent, laterally extensive, and widely spaced. Butt cleats constitute a poorly defined set of natural fractures, orthogonal or nearly orthogonal to

**Fig. 1** Digital representation of an RGB image [33]



face cleats. The complex cleat system intersects within coal seam and leaves a blocky structure.

Furthermore, the brightness is another important feature of coal. Macro-lithotype has been used to define the physical and mechanical properties of coals [35–37]. The coal lithotype is determined based on the megascopically visible feature of a coal bed, including the percentage of brightness and texture. Bright coal has well developed cleats, while dull coal has wider cleat spacing. Since cleating is higher in brighter coal bands, the use of the terms “bright” and “dull” infers a measure of volumetric cleat density [37]. Although the classification of coal lithotype is not within the scope of this study, the brightness profile of coal provides a unique feature for rock and coal classification.

Shale, siltstone, and sandstone are the common coal measures rocks observed within the coal seam horizon as rock partings, mine roof, or mine floor. They are all clastic sedimentary rocks made up of particles of different sizes. Shale is mostly made of clay-size grains, siltstone is formed from silt-size grains while sandstone is made of sand-sized clasts. The sediments are deposited in layers, forming a bedding structure. In addition, due to the varying component of organic matter, the color can vary from gray to black. However, due to the absence of a cleating system, no brightness profile can be visually observed.

Finally, the above analyses indicate that color, grain size and distribution, structure (cleat and bedding), and reflectance are important features to classify coal and other coal measures rocks. However, the unfavorable conditions, including low illumination and dusty air, make it difficult to visualize the grain size and distribution in digital images created under operational conditions. Therefore, the color, structure, and brightness become the key features to visually classify coal and other coal measures rocks on images. They are the general features for visually classifying rock and coal in underground coal mines. Due to the difference in color and brightness, different pixel values may be observed

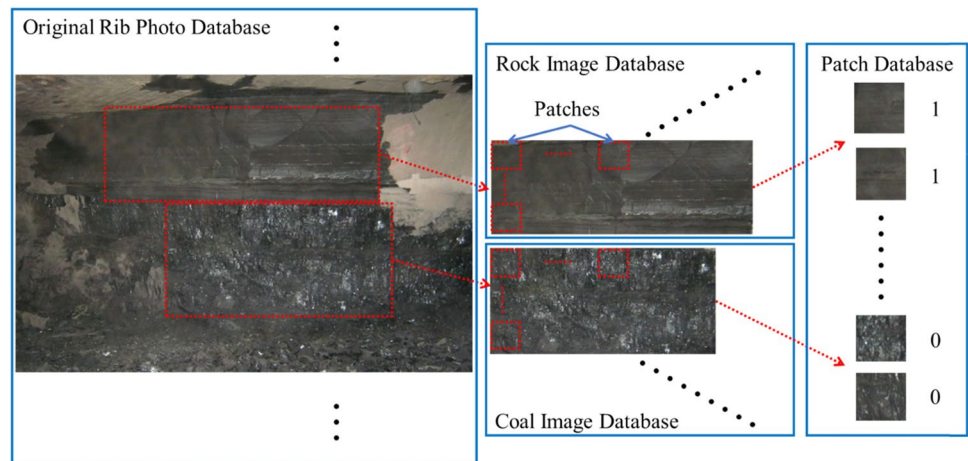
between coal and other rocks; due to the different structures, different textures or patterns in the pixel values may be observed within a local area. These are the potential mechanisms for classifying rock and coal with digital images.

### 2.3 Image Database

In order to control rib failures in underground coal mines, NIOSH is developing a coal rib stability rating technique to characterize the bearing capacity of coal ribs [1]. Photos have been taken by researchers to capture the failure mode of coal ribs during the extensive field trips to underground coal mines in the USA. Within some photos, rock and/or coal can be observed from the fresh failure surfaces. These photos were selected to generate the rock and coal image database. It is worth noting that these photos were collected from different sources and they were taken with different illuminations, subject distances, focal lengths, and angles. They cover a wide range of coal and rocks under different conditions observed in underground coal mines.

Most of the rocks on ribs in gateroads are either weathered or covered with rock dust and sealant, which significantly affects the color and structure. In order to obtain the representative features of coal and rock, the areas with fresh surface within the photos were selected for this study. The processing of rib images is shown in Fig. 2. On the rib image, the fresh areas of rock and coal were manually selected within rectangular boxes via the Windows Snipping tool. In this way, the cropped images with varying sizes have the same resolution and were organized to generate the rock and coal image database. As shown in Fig. 2, smaller images, namely, patches, were further extracted from each rock or coal image to generate a rock and coal patch database. Since hundreds or thousands of patches can be extracted from each image, the patch database is much larger than the rock and coal image database. The machine learning process is based on the patches. As discussed earlier, the RGB images are

**Fig. 2** Image processing to generate the database





stored as three-dimensional arrays, and the extraction of patches is accomplished by extracting subarrays.

Examples of the collected rock and coal images are shown in Fig. 3. The image database only contains the areas with fresh surface on the ribs, which are normally generated due to rib failure of various sizes. As a result, rectangular images with various sizes were cropped manually from the original photos. The irregular fresh surface, bolts, and wires on the rib images also restricted the areas that can be cropped. Furthermore, the areas that we are interested in may not be the focused areas when taking the photos, and thus the quality of the cropped images can be poor. Due to the angle, illumination, and varying distances, the cropped images may not be able to show all the features of the areas of interest. However, the rock and coal can be classified by the original photos with the naked human eye. Even if some features are shaded by the angle and light, classification can still be achieved based on the visually observable features, and it is expected that the machine learning model could achieve that as well. Thus, all the fresh areas that can be identified as rock and coal on the ribs are cropped and included in the database, regardless of the quality of the photos. There were even areas that cannot be identified with naked eyes but can be inferred from the extent of the rock or coal stratum. These areas were included in the database to aid in determining the capacity of the machine learning model. Therefore, the

rock and coal database include images of different sizes and qualities. It is expected that the database could cover a wide range of the complicated situations that appear when taking photos or capturing images from videos. As summarized in Table 1, a total of 71 images and 97 images were obtained for the coal and rock database, respectively.

The cropped images in the database have different sizes and contain different amounts of information for the rock and coal. After importing the images with Scikit-Image package [38], the *PatchExtractor* function of Scikit-Learn package was used to extract patches from each image [39]. The purpose for patch extraction is to generate a large number of images of the same size for analysis. The feature extraction and classification are conducted on the patches. When training the classifier, patches with a given size can be used. When the trained model is used to classify rock and coal, images of the same size as the patches should be

**Table 1** Summary of the image database

Type	Number of original images	Number of cropped images	Patch size (pixel)	Number of patches
Coal	87	71	50*50	10,650
Rock		97		14,550

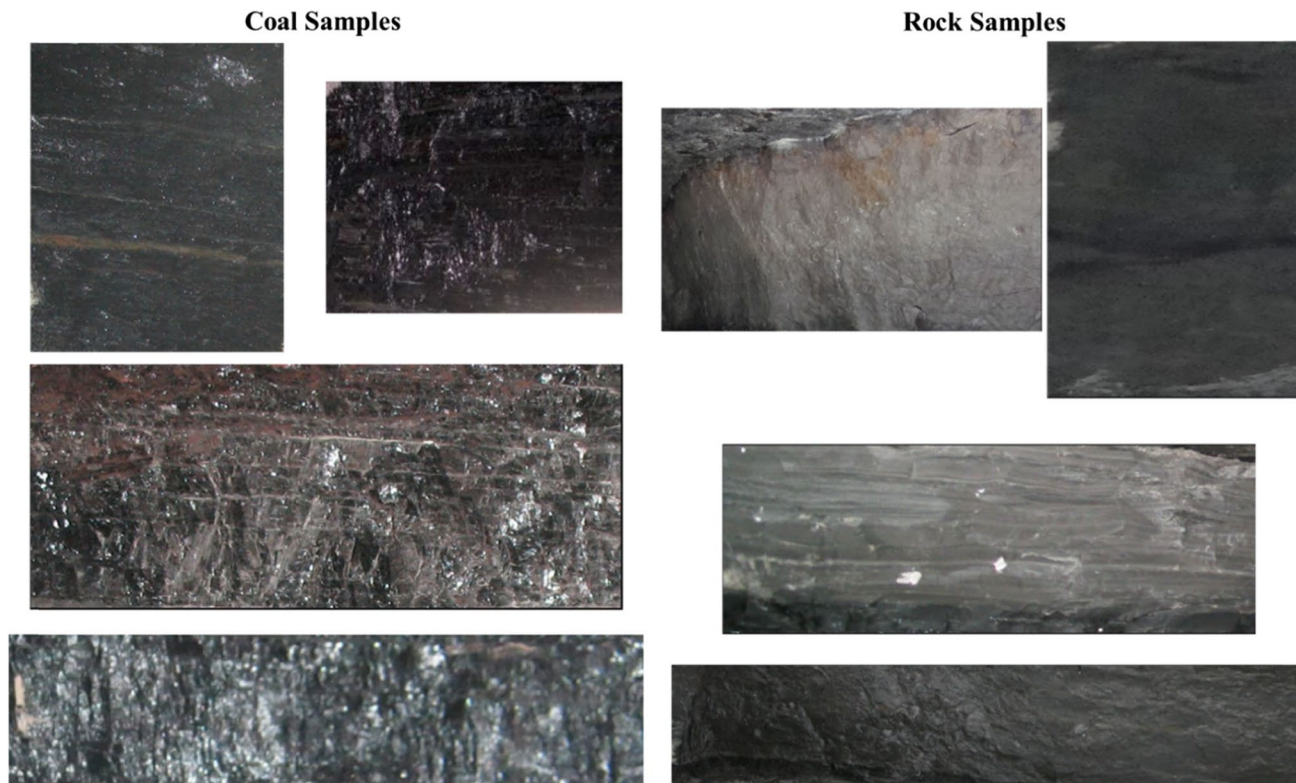


**Fig. 3** Examples of collected rock and coal images

used. Otherwise, a lack of accuracy could be the outcome. However, it is critical to choose the patch size. If the patch is too large, it may be inaccurate for identifying a thin rock layer within the coal seam. If the patch is too small, it may not be able to capture enough features of rock and coal. At this point, a patch size of 50\*50 in pixels was used. A comparison study on the patch size was conducted to optimize the patch size in the following section.

Besides the patch size, the *PatchExtractor* function could assign a maximum number of patches that can be extracted from each image. Since images of different sizes were used in this study, the maximum number was used to prevent the predominant influence of large images, which were taken under a specific condition or captured a specific rock type. For a determined patch size, large images can extract more patches than the small ones, and as a result, the features of the large images play a predominant role for coal or rock and the unique features showing on the small images may be ignored. In order to prevent this situation, same number of patches needs to be extracted from each image. After trial and error on a computer with 32 GB RAM, a maximum number of 150 patches was used. This means that 150 patches would be randomly extracted from each rock or coal image. In this way, the total number of patches was restricted, and each image made the same contribution to the collection of patches. The database for the images and patches is summarized in Table 1. Even though the number of patches extracted from each image was limited to 150, there were still 10,500 and 14,550 patches extracted for coal and rock, respectively. Therefore, a total of 25,050 patches, each with 7500 pixel values, were obtained for model training and validation.

### 3 Machine Learning Model

#### 3.1 Model Training, Tuning, and Validation with Support Vector Machine

The cropped images for rock and coal were originally stored in two folders in this study. Each image of each folder was imported and then fed into the patch-extraction function to extract the patches, which were represented as three-dimensional arrays. The patch data were stacked to form a dataset for rock and coal, respectively. The patch data are the feature arrays. At the same time, the label of “1” and “0” were provided in a target array to represent rock and coal, respectively. Rock is normally the minor part within the images and the purpose of this study is to classify rocks from the rib images. As a result, the rock patches were labeled as “1” and were treated to be positive cases; the coal patches were labeled as “0” and were treated as negative cases. Then, each dataset was randomly split into a training set and a testing

set. The training dataset contains 75% of the total data and was used to train the model so that the classifier could identify the features for classifying coal and rock. The remaining 25% of the data was used to check the performance of the trained classifier.

Various machine learning techniques from the Scikit-Learn package were used to process the data [39]. Dimensionality reduction technique was used to preprocess the images data. The patch size of 50\*50 pixels with three color channels led to 7500 pixel values for each patch. If each pixel value was used as a feature, the data for each patch is 7500-dimensional. However, a more efficient way is to use a preprocessor to extract some more meaningful features. Principal component analysis (PCA) is such a method, which is fundamentally a dimensionality reduction technique and is useful as a tool for visualization, for noise filtering, for feature extraction and engineering, and much more [40]. PCA simply projects the data onto the principal axes and measures the importance of each feature. The information along the least important principal axes is removed, leaving only the components with the highest variance. In this way, PCA filters some noise and removes less important features and the goal is to represent the data in a suitable lower dimension and retain the essential features of the data. It has been used for the identification of coal textures in different rock coal reservoirs with geophysical logging data [41].

Support vector machine (SVM) was used as the classifier. It is a discriminative classifier formally defined by a separating hyper-plane or a set of hyper-planes in a high- or infinite-dimensional space. In two-dimensional space, the hyper-plane is a line dividing the data into two parts where each class lay in either side. It has been widely used for classification problems and good accuracy has been achieved for different problems [42–47]. Another advantage of SVM is the processing time. Compared with other classifiers, it takes a shorter amount of time, potentially making it possible to recognize the rock/coal interface at longwall face in real time.

In addition, the PCA preprocessor and SVM classifier could be further packaged into a single pipeline, which sequentially applies a list of transforming operations and a final classifier. In machine learning, there are different transformations (filling missing values, feature engineering, and dimensionality reduction) of raw data before applying the data to the final classifier. Using PCA to reduce the dimension of the data is such a transformation. With pipeline, all of these procedures can be combined in sequence. When some new raw data is provided, the pipeline preprocesses the data and feeds the processed data into the classifier for prediction, automating the prediction process of machine learning.

Furthermore, a grid search cross-validation method was used to tune the hyper-parameters for the classifier. The

process is shown in Fig. 4. There are various hyper-parameters controlling the training process of the classifier and further affecting its performance. The grid search cross-validation method allows the search of best hyper-parameters by exploring different combinations of the hyper-parameters. The cross-validation method involves randomly splitting the dataset into K groups (5, by default). For each iteration, one group of data is used as validation data, while the remaining groups are taken as training data. The classifier with one group of hyper-parameters is fitted with the training data and is evaluated with the testing data to get an evaluation score. After K iterations, the average evaluation score is used to quantify the performance of the hyper-parameter combination. After obtaining the average evaluation score for all the hyper-parameter combinations, the best hyper-parameters can be selected. Since PCA and the classifier were packaged into a single pipeline, the hyper-parameters for PCA and the classifier were optimized together. Specifically, the number of fundamental components was 100 as the best hyper-parameter for PCA. It means that PCA would extract 100 components from the 7500 features for the training and testing.

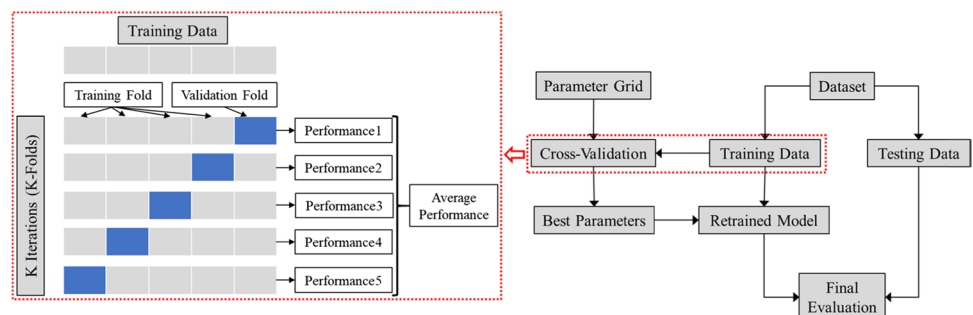
In order to evaluate the performance, the trained classifier with tuned hyper-parameters was further used to classify the rock and coal patches from the testing dataset. There are various approaches to evaluate the performance of a classifier. A confusion matrix is a table illustrating the classifier performance, and various scores can also be used to evaluate the classifier. As shown in Table 2, the accuracy score is the ratio of the correctly predicted observation to the total observations, and recall score is the ratio of correctly predicted

positive observations to all observations in the positive class. For the classification of rock and coal, the rock patches were treated to be positive, and the coal patches were treated as negative cases. As a result, in Table 2, the false-positive cases are coal which were classified to be rock; while false-negative cases are rock which were classified as coal.

The confusion matrix and scores for the SVM classifier are shown in Table 3. From the confusion matrix, we can see that there were 627 wrong predictions and a total of 5636 cases were predicted correctly. An accuracy score of 0.900 was obtained. At the same time, there were 295 false-negative cases and 3316 true-positive cases, leading to a recall score of 0.918. The high accuracy score and recall scores demonstrate the capability of the classifier in classifying rock from coal.

Some examples of the wrong predictions, false-positive and false-negative cases, are plotted in Fig. 5. We can see that they all have low visibility, especially for all false-positive cases and the left three false-negative cases. Due to the inclined angles between the surface and light and between the surface and camera lens, the features of the surface become less visible on the far side. It is even difficult to classify with naked eyes. From the extent of the rock or coal stratum, it was inferred that a specific area was rock or coal even without visible features, which normally occurred on the far side of an image. In order to determine the capability of the classifier, rather than increase the accuracy with only clear images, these kinds of areas with low visibility and inferred type (rock or coal) were also included in the database. The accuracy of the model was reduced when these areas were randomly extracted as patches for training and

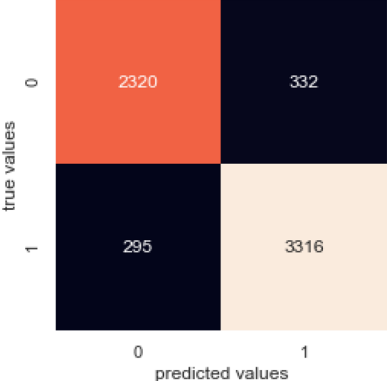
**Fig. 4** Machine learning with the grid search cross-validation method

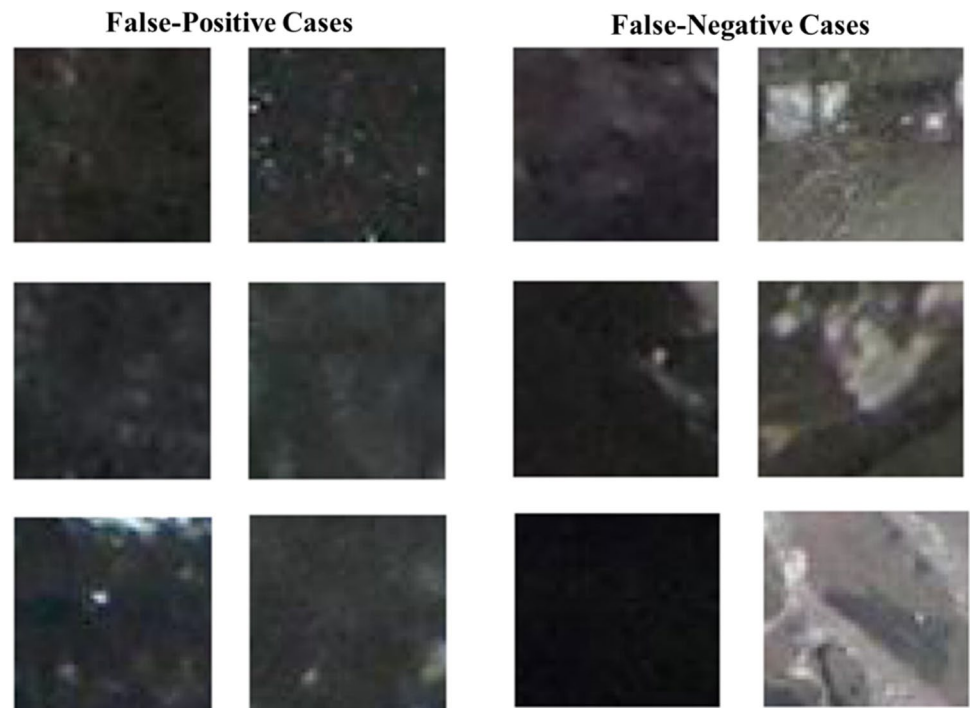


**Table 2** Model performance evaluation definition

True Values 0 (Coal) 1 (Rock)	True Negative (TN)	False Positive (FP)	Accuracy Score	$\frac{TN + TP}{TN + FP + FN + TP}$
	False Negative (FN)	True Positive (TP)		
Predicted Values 0 (Coal)      1 (Rock)			Recall Score	$\frac{TP}{FN + TP}$

**Table 3** Performance of the SVM model

	Accuracy Score	0.900
	Recall Score	0.918

**Fig. 5** Examples of the wrong predictions (false-positive cases are coal but are classified as rock; while false-negative cases are rock but are classified as coal)

testing. In addition, some other materials, neither coal nor rock, attached on the surface may have affected the accuracy. The right three false-negative cases fall into this category. In order to crop rock and coal images as large as possible, small areas covered with other materials, for example sealant, may have been included in the image database. When patches with a size of 50\*50 pixels were extracted from the images, the contribution of these areas to the features of the patches (color and texture) may be significant enough to affect the results.

### 3.2 Influence of Patch Size on Accuracy

The patch size is one factor potentially affecting the accuracy of the classifier. If the patch is too small, it may be incapable

of capturing essential features of the objects. The accuracy of a classifier trained to detect an object will be questionable when the model is trained with images covering only a small portion of the object. On the other hand, if the patch is too large, it may include repeating information and thus increase the processing and calculation work. In addition, the large patches potentially cover both rock and coal when the classifier is applied to classify rock and coal from an original rib image. Due to the minor influence on the image features, the minor part, either rock or coal, is potentially being neglected by the classifier, leading to missing thin rock or coal layer from the prediction.

In order to determine the influence of patch size on accuracy, different patch sizes were used to train and test the classifier. When selecting the patch size, the minimum size



of the rock and coal image was taken into consideration. The minimum dimension of the rock and coal images was 126 pixels. In order to get enough patches, a maximum patch dimension of 100 pixels was used. The studied patch size included 25\*25, 50\*50, 75\*75, and 100\*100 pixels. The maximum number of patches extracted from each image was fixed at 150. This made the total number of patches the same for varying patch sizes.

Learning curves were used to monitor the cross-validated training and testing scores of the model with varying training sizes. It is a tool to find out how the model responds to increasing training data and whether the model suffers from a variance error or a bias error. Similar to the cross-validation process in Fig. 4, the training data is randomly separated into K folds. The default value for K is 3 here, and thus, the training data has one validation fold and two training folds. Subsets of the training folds with varying sizes (10.0%, 32.5%, 55.0%, 77.5%, and 100% of the training folds, by default) are used to train the classifier, and a score for each training subset size and the validation data are calculated. Since the cross-validation is threefold, three training scores and three testing scores will be obtained for each training size, and the learning curve shows the average score and standard deviation with different training sizes. The learning curves with different patch sizes are plotted in Fig. 6. It is observable that all the curves are converging with the increase in training size. The training score for the model trained with patches of 25\*25 and 50\*50 pixels gradually decreases within increasing training size, while the other two models show ignorable change in the training score. However, all training curves gradually converge. At the same time, all the testing scores gradually increase and converge with the increasing size of the training dataset. The converging scores indicate that adding more training data will not significantly improve the accuracy.

In addition, the testing curves in Fig. 6b show that the testing scores gradually converge to different values for varying patch sizes. The general trend is that larger patch size leads to higher testing score. However, the difference in the testing scores decreases with the increasing patch size. There is significant difference between the patch size of 25\*25 and the other three, while the difference between the other three are minor. Especially for the patch size of 75\*75 and 100\*100, the testing curves almost overlap with any training size. This indicates that, for the rock and coal image database, a size of 75\*75 pixels is a representative patch size to include essential rock and coal features, and there will be no more increase in the accuracy if the patch size further increases.

It should be noted that this is concluded for the patches extracted from two separated datasets where the patches are “purely” coal or rock but may not be exactly applicable for patches with both rock and coal. When the classifier is used

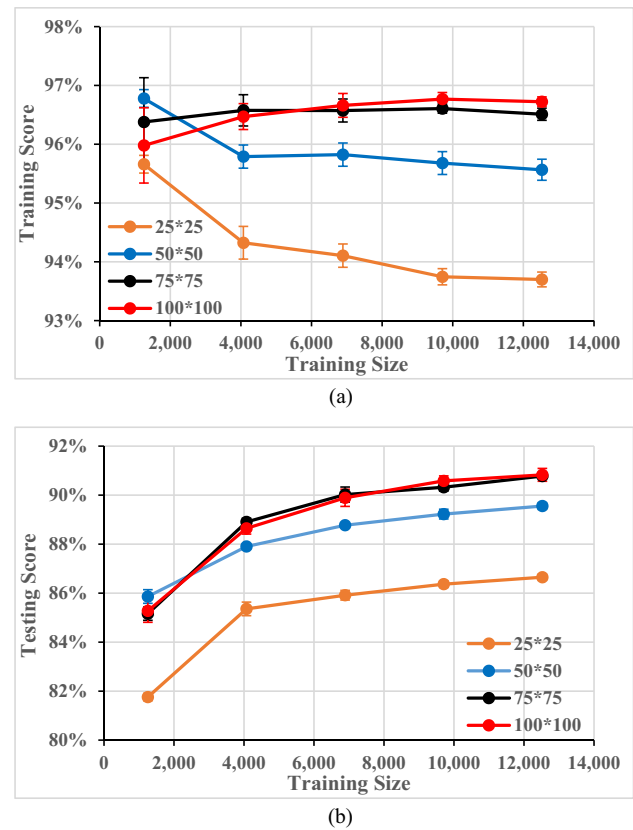


**Fig. 6** Learning curves for the model with different patch sizes. **a** Training score. **b** Testing score

to detect rock from coal on a rib image, the extracted patches may cover rock and coal at the same time, potentially affecting the accuracy. Larger patches have a higher possibility to come into this situation and the higher accuracy cannot be guaranteed.

### 3.3 Influence of Machine Learning Models

Another factor affecting prediction accuracy is the classifier. The classifiers are based on different statistical methods and potentially obtain different accuracies. A second classifier was used for rock and coal classification with rib images and was compared with the SVM classifier. The Random Forest (RF) model has been widely used in machine learning projects for rock mechanics and rock engineering, and fast processing speed and good accuracy are achieved with this model [42, 45, 48–50]. Therefore, the Random Forest model of Scikit-Learn package was selected for this classification problem [39]. It constructs several decision tree classifiers on various subsets of the dataset and uses averaging to improve the predictive accuracy and control over-fitting.

Similarly, the PCA preprocessor and the RF classifier were packaged into a single pipeline. The original data was preprocessed with PCA to reduce the dimensions and

then was fed into the classifier for training and testing. The grid search cross-validation method was used to optimize the hyper-parameters and the result showed that the best performance was achieved with the number of fundamental components of 100 for PCA, which was the same as the pipeline with the SVM classifier. After training with 75% of the patches, the classifier was evaluated with the rest of the patches. The performance of the RF classifier is summarized in Table 4. Compared with the performance of the SVM model in Table 3, there are 19 less false-negative cases and 2 more false-positive cases with the RF classifier. The slight change in the wrong predictions leads to an ignorable change in the accuracy score and recall score.

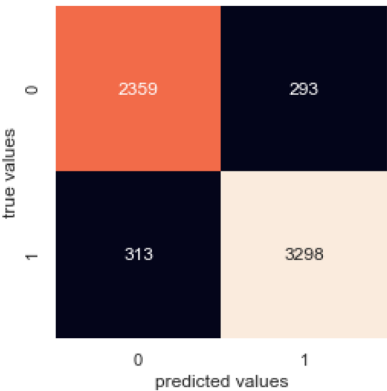
## 4 Application

The ultimate purpose of this study is to identify rocks within coal ribs through the classification of extracted patches from input rib images. The method used for face detection was applied in this study. For face recognition, it is impractical to analyze the whole screen. Only analyzing the patch covering a face is necessary for recognition purpose. One method to detect a face within an image is to extract patches from the image and analyze each patch with a trained classifier [40]. The classifier was previously trained with images with and

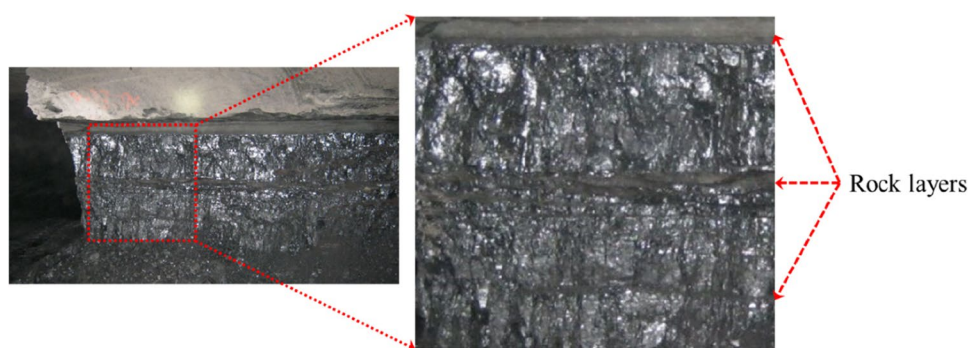
without faces and the features of faces had already been captured by the classifier. Each patch was analyzed by the classifier to verify whether there is a face. In such a way, the face(s) on a large image can be detected and can be used for recognition with another classifier. Similarly, a classifier that was trained to classify rock and coal can be used for the patches extracted from a rib image. All the patches identified to be rock can be highlighted to form a rock layer on the rib.

The rib image used for the application is shown in Fig. 7. The image was not used in the previous training and testing process. It is a new image for the model. Part of the image with fresh surface was cropped and imported. The input image has 732 and 782 pixels in the horizontal and vertical direction, respectively. A sliding window function was used to extract small patches from the input image [40]. The enlarged view of the input image in Fig. 7 shows that there are three layers of rock partings with decreasing thickness from the top to the bottom. In order to capture the thin rock layers, a patches size of 50\*50 pixels was used for the application. We can see from Fig. 6b that there is a slight reduction in the testing score when the patch size reduces from 75\*75 pixels to 50\*50 pixels. However, it is believed that the reducing patch size assists in capturing thin rock layers. The small sliding windows have an offset of 10 pixels in both the horizontal and vertical direction, leading to a total number of patches of 5106. The 5106 arrays, each with 7500

**Table 4** Performance of the RF classifier

	Accuracy Score	0.903
	Recall Score	0.913

**Fig. 7** The rib image used for model application



values, were fed into the pipelines to conduct dimensionality reduction and make predictions.

The predicted results are shown in Fig. 8. The patches that were predicted to be rock are marked with red border on the input image. Figure 8a shows the result predicted with the SVM classifier, and we can see that the approximate locations of the three rock layers could be identified from the rock patches. However, the accuracy depends on patch size and rock layer thickness. The top layer has the maximum thickness and the whole layer is accurately predicted. The patches overlap and cover the top rock parting. With reducing thickness, there is less overlapped rock patches, which cannot cover the whole rock layer. This resulted from less contribution of the rock layer to the whole patch with a determined size of 50\*50 pixels. Smaller patch size may assist in identifying the thinner rock partings. However, further reducing the patch size could decrease the accuracy, as shown in Fig. 6b and increase the number of patches to analyze as well. In addition, the purpose is to identify the rock layer in a timely manner, and a patch offset of 10 pixels was used, which helped to reduce the number of patches to analyze. However, this potentially leads to less overlapped rock patches for the thin rock layers.

Another important concern for rock and coal classification at the mining face is the time taken to preprocess the image and to classify rock and coal. The time taken for this application problem was determined with Python functions. The results show that it took 46.9 ms to extract 5106 patches from the input image, 172 ms to reshape the arrays, and 3.11 s to classify the 5106 patches with the SVM classifier. Thus, the total time taken to classify rock and coal on the input image with 732\*782 pixels was about 3.33 s. From a time-consuming point of view, it is practical for the proposed method to classify rock and coal at the mining faces in real time. If the purpose is to identify the immediate roof for automated shearers cutting, only the top part of the rib

image needs to be analyzed and the time cost can be further reduced.

Compared with the SVM classifier, the processing time for the RF classifier to classify the 5106 patches was 297 ms, which was much faster than the SVM. However, the comparison between the predicted results in Fig. 8 shows that the SVM classifier shows better accuracy for this application problem, especially for the central and bottom thin rock layers.

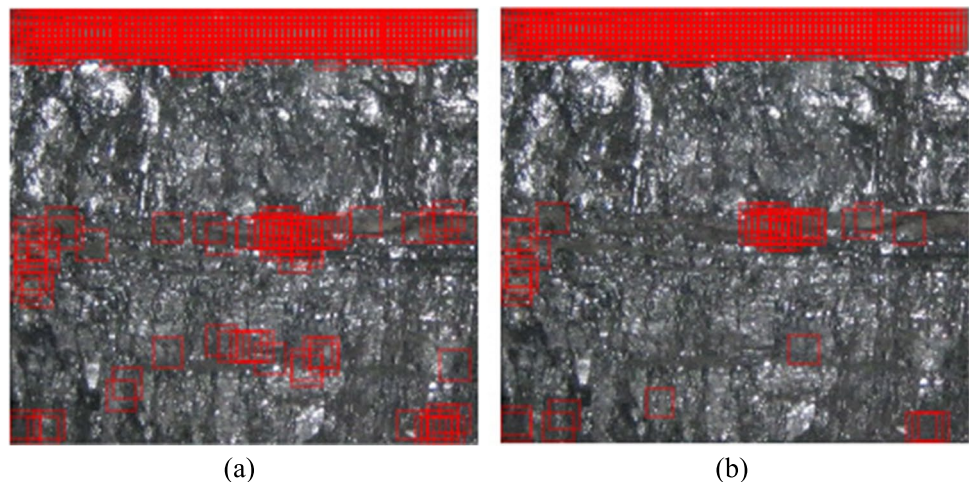
This shows a simple application of the classifier to classify the rock and coal on an image and much more improvement can be achieved. On one hand, the method only searches with one patch size. If the thickness of the rock layer is much smaller than the patch size, the method may make a wrong classification. Different patch sizes could be used for the training and application to capture the thin rock layers. On the other hand, there are overlapped patches for the rock layer, which are not preferred. Some other techniques may be used to further reduce the overlapped detections and determine the thickness of the rock layers.

## 5 Conclusions

Classification of rock and coal in real time assists in automated coal rib rating and enables shearers to adjust the drum automatically without human intervention. Machine learning techniques were used to classify rocks from coal based on rib images in gateroads. Some conclusions can be drawn from this study.

The difference in composition and sedimentary environment provides some unique features to classify coal and other coal measures rocks. Due to the unfavorable photo-taking condition in underground coal mines, grain size and distribution cannot be captured, while color, structure, and brightness can be used to classify rock and coal. The

**Fig. 8** Predicted results with different classifiers. **a** SVM. **b** RF



difference in the features is reflected in the pixel value and is analyzed by the machine learning model.

In addition, good accuracy was obtained for the trained classifier. After training, the classifier was validated with the testing dataset and an accuracy score of 0.9 was obtained. Similar accuracy scores were obtained with the SVM and RF classifiers. The study on the patch size shows that a patch size of 75\*75 pixels can be used as the representative patch size for training and testing purposes. Further increasing patch size may not significantly improve the model accuracy and would increase the data volume to process.

Furthermore, the trained classifier was applied to classify rocks from a coal rib image. Patches were extracted from the rib image and were analyzed with the classifier. The highlighted rock patches illustrate the approximate location of the three rock layers with different thicknesses. However, the accuracy depends on the rock layer thickness and patch size. With a patch size of 50\*50 pixels, the classifier successfully captured the thick rock layer with overlapped rock patches. The accuracy gradually decreased with reducing rock layer thickness, resulting from less contribution of the rock layer within the patch. The extracting and classifying thousands of patches only took seconds, making it a practical method for the classification of rock and coal in real time.

#### Declaration

**Conflict of Interest** On behalf of all authors, the corresponding author states that there is no conflict of interest.

## References

- Mohamed KM, Van Dyke M, Rashed G, Sears MM, Kimutis R (2020) Preliminary rib support requirements for solid coal ribs using a coal pillar rib rating. 39th Int. Conf. Gr. Control Min., Canonsburg, PA, USA: 85–96.
- Bauer BER, Dolinar DR (1999) Skin Failure of Roof and Rib and Support Techniques in Underground Coal Mines. 18th Int. Conf. Gr. Control Min., Morgantown, WV USA: 99–109.
- Colwell MG (2004) Analysis and design of rib support (ADRS)-Rib support design methodology for Australian Collieries. ACARP Project C11027
- Mark C, Pappas DM, Barczak TM (2009) Current trends in reducing groundfall accidents in U.S. coal mines. 2009 SME Annu. Meet. Exhib., vol. 63, Littleton, CO, USA: 22–5
- Pappas DM, Mark C (2012) Roof and rib fall incident trends: a 10-year profile. Trans Soc Mining, Metall Explor 330:462–478
- Jones TH, Mohamed KM, Klemetti TM (2014) Investigating the contributing factors to rib fatalities through historical analysis. 33rd Int. Conf. Gr. Control Min., Morgantown, WV, USA: 113–23
- Zhang P, Mohamed KM, Trackemas J (2017) Coal rib failure and support in longwall gate entries. 51st US Rock Mech / Geomech Symp 2017 5:3154–3164
- Rashed G, Mohamed KM, Gearhart DF, Esterhuizen GS (2019) Calibration of coal-mass model in a longwall mine : a case study. 53rd US Rock Mech. Symp., New York City, NY USA
- Ralston JC, Hargrave CO, Dunn MT (2017) Longwall automation: trends, challenges and opportunities. Int J Min Sci Technol 27:733–739. <https://doi.org/10.1016/j.ijmst.2017.07.027>
- Mohamed KM, Cheng Z, Rashed G (2019) Coal rib stability based on the strength reduction of the coal mass model. 53rd U.S. Rock Mech. Symp., New York City, NY USA
- Mohamed K, Xue Y, Rashed G, Kimutis R (2021) Analyzing rib stability and support using a coal pillar rib rating. 40th Int. Conf. Gr. Control Min
- Xue Y, Mohamed K (2021) Investigating the factors affecting the stability of coal ribs with in-seam partings through numerical simulations. 40th Int. Conf. Gr. Control Min
- Peng SS (2019) Automation of longwall components and systems. Longwall Min. 3rd Ed., CRC Press:308–35
- Peng SS, Du F, Cheng J, Li Y (2019) Automation in U.S. longwall coal mining: A state-of-the-art review. Int J Min Sci Technol 29:151–9. <https://doi.org/10.1016/j.ijmst.2019.01.005>
- Nelson MG (1989) Simulation of boundary coal thickness sensors, Doctoral dissertation, West Virginia University
- Ralston JC, Reid DC, Dunn MT, Hainsworth DW (2015) Longwall automation: Delivering enabling technology to achieve safer and more productive underground mining. Int J Min Sci Technol 25:865–876
- Wang H, Huang X, Zhao X, Liang Z, Housein AAl, Shao Q, et al (2019) Dynamic coal-rock interface identification based on infrared thermal image characteristics. 2019 IEEE 3rd Inf. Technol. Networking, Electron. Autom. Control Conf., Chengdu, China: 589–96
- Wang H, Zhang Q (2019) Dynamic identification of coal-rock interface based on adaptive weight optimization and multi-sensor information fusion. Inf Fusion 51:114–128
- Miao S, Liu X, Liu Z, Zhang L, Zhang K (2018) Ground penetrating radar based experimental simulation and signal interpretation on coal-rock interface detection. IOP Conf Ser Mater Sci Eng 439:0–7. <https://doi.org/10.1088/1757-899X/439/5/052018>.
- Rao AR, Lohse GL (1996) Towards a texture naming system: Identifying relevant dimensions of texture. Vision Res 36:1649–1669
- Partio M, Cramariuc B, Gabbouj M, Visa A (2002) Rock texture retrieval using gray level co-occurrence matrix. In Proc. of 5th Nordic Signal Processing Symposium (Vol. 75)
- Sun J, Su B (2013) Coal-rock interface detection on the basis of image texture features. Int J Min Sci Technol 23:681–687
- Lepistö L, Kunttu I, Autio J, Visa A, Box PO (2004) Tampere F-. Rock image retrieval and classification based on granularity. 5th Int. Image Anal. Multimed. Interact. Serv., Lisboa, Portugal
- Lepistö L, Kunttu I, Visa A, Autio J. Retrieval of non-homogenous textures based on directionality. 107–110. [https://doi.org/10.1142/9789812704337\\_0020](https://doi.org/10.1142/9789812704337_0020)
- Lepistö L, Kunttu I, Autio J, Visa A (2003) Classification method for colored natural textures using Gabor filtering. Proc - 12th Int Conf Image Anal Process ICIAP 2003:397–401. <https://doi.org/10.1109/ICIAP.2003.1234082>
- Crelling JC (1982) Automated petrographic characterization of coal lithotypes. Int J Coal Geol 1:347–359. [https://doi.org/10.1016/0166-5162\(82\)90020-9](https://doi.org/10.1016/0166-5162(82)90020-9)
- Unsworth JF, Gough H (1989) Characterization of coals by automated optical image analysis 1. Vitrinite reflectance J Microsc 156:313–326
- Lee JB (1985) Image analyser measurements of coal reflectance. J Microsc 137:145–154
- Yu K, Barry JC, Esterle JS (1997) Analysis of coal banding texture and implications for megascopic image analysis. Int J Coal Geol 33:1–18. [https://doi.org/10.1016/S0166-5162\(96\)00022-5](https://doi.org/10.1016/S0166-5162(96)00022-5)



30. Samuel AL (1959) Some studies in machine learning using the game of checkers. *IBM J Res Dev* 3:210–229
31. Géron A (2017) Hands-on machine learning with Scikit-Learn, Keras, and TensorFlow: Concepts, tools, and techniques to build intelligent systems. O'Reilly Media
32. Ran X, Xue L, Zhang Y, Liu Z, Sang X, He J (2019) Rock classification from field image patches analyzed using a deep convolutional neural network. *Mathematics* 7:1–16. <https://doi.org/10.3390/math7080755>
33. Wallpaper for desktop-natural stones in different colors n.d. [wallpapers13.com/natural-stones-in-different-colors-red-green-blue-and-white-color-wallpaper-for-desktop/](https://wallpapers13.com/natural-stones-in-different-colors-red-green-blue-and-white-color-wallpaper-for-desktop/) (accessed February 2, 2020).
34. Rodrigues CF, Laiginhas C, Fernandes M, Lemos de Sousa MJ, Dinis MAP (2014) The coal cleat system: A new approach to its study. *J Rock Mech Geotech Eng* 6:208–18. <https://doi.org/10.1016/j.jrmge.2014.03.005>
35. Zhao J, Xu H, Tang D, Mathews JP, Li S, Tao S (2016) Coal seam porosity and fracture heterogeneity of macrolithotypes in the Hancheng Block, eastern margin, Ordos Basin. *China Int J Coal Geol* 159:18–29. <https://doi.org/10.1016/j.coal.2016.03.019>
36. Rusnak JA (2017) Coal strength variation by lithotype for high-volatile A bituminous coal in the central Appalachian Basin. *Proc. 36th Int. Conf. Gr. Control Min., Morgantown, WV USA: 198–207*
37. Rashed G, Barton T, Sears M, Van Dyke M, Mohamed K, Dyke M van, et al (2018) Estimation of the intact strength of coal using indirect methods. *Proc. 37th Int. Conf. Gr. Control Min., Morgantown, WV, USA: 294–301*
38. van der Walt S, Schönberger JL, Nunez-Iglesias J, Boulogne F, Warner JD, Yager N et al (2014) scikit-image: Image processing in Python. *PeerJ* 2:e453
39. Pedregosa F, Varoquaus G, Gramfort A, Michel V, Thirion B, Grisel O (2011) Scikit-learn: Machine Learning in Python. *J Mach Learn Res* 12:2825–30
40. VanderPlas J (2016) Python data science handbook: Essential tools for working with data. “O'Reilly Media, Inc.”
41. Ren P, Xu H, Tang D, Li Y, Sun C, Tao S et al (2018) The identification of coal texture in different rank coal reservoirs by using geophysical logging data in northwest Guizhou, China: Investigation by principal component analysis. *Fuel* 230:258–265. <https://doi.org/10.1016/j.fuel.2018.05.019>
42. Zhou J, Li X, Mitri HS (2015) Comparative performance of six supervised learning methods for the development of models of hard rock pillar stability prediction. *Nat Hazards* 79:291–316. <https://doi.org/10.1007/s11069-015-1842-3>
43. Kumar M, Aiyer BG, Samui P (2014) Machine learning techniques applied to uniaxial compressive strength of oporto granite. *Int J Performability Eng* 10:189–195
44. Zhou Z, Cheng R, Cai X, Ma D, Jiang C (2018) Discrimination of Rock Fracture and Blast Events Based on Signal Complexity and Machine Learning. *Shock Vib* 2018. <https://doi.org/10.1155/2018/9753028>.
45. Zhou J, Li X, Mitri HS (2016) Classification of rockburst in underground projects: Comparison of ten supervised learning methods. *J Comput Civ Eng* 30. [https://doi.org/10.1061/\(ASCE\)CP.1943-5487.0000553](https://doi.org/10.1061/(ASCE)CP.1943-5487.0000553)
46. Xu H, Zhou J, Asteris PG, Armaghani DJ, Tahir MM (2019) Supervised machine learning techniques to the prediction of tunnel boring machine penetration rate. *Appl Sci* 9:1–19. <https://doi.org/10.3390/app9183715>
47. Peng YH, Peng K, Zhou J, Liu ZX (2014) Prediction of classification of rock burst risk based on genetic algorithms with SVM. *Appl Mech Mater* 628:383–389. <https://doi.org/10.4028/www.scientific.net/AMM.628.383>
48. Ding H, Li G, Dong X, Lin A (2018) Prediction of pillar stability for underground mines using the stochastic gradient boosting technique. *IEEE Access* 6:69253–69264
49. Lin Y, Zhou K, Li J (2018) Prediction of slope stability using four supervised learning methods. *IEEE Access* 6:31169–31179. <https://doi.org/10.1109/ACCESS.2018.2843787>
50. Qi C, Fourie A, Du X, Tang X (2018) Prediction of open stope hangingwall stability using random forests. *Nat Hazards* 92:1179–1197

**Publisher's Note** Springer Nature remains neutral with regard to jurisdictional claims in published maps and institutional affiliations.